INVESTIGATION OF CARRIER TRANSPORT IN SURFACE BARRIER DEVICES ON POLYSILICON

By

K. M. PANCHAL
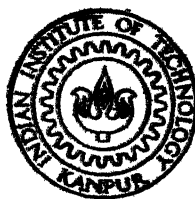
INTERDISCIPLINARY PROGRAMME IN MATERIALS SCIENCE

INDIAN INSTITUTE OF TECHNOLOGY KANPUR

AUGUST, 1980

INVESTIGATION OF CARRIER TRANSPORT IN SURFACE BARRIER DEVICES ON POLYSILICON

A Thesis Submitted
in Partial Fulfilment of the Requirements
for the Degree of
MASTER OF TECHNOLOGY

By
K. M PANCHAL

to the
INTERDISCIPLINARY PROGRAMME IN MATERIALS SCIENCE
INDIAN INSTITUTE OF TECHNOLOGY KANPUR
AUGUST, 1980

IPMS-1980-M-PAIN -INV

CERTIFICATE

This is to certify that the thesis entitled
" Investigation of Carrier Transport in Surface Barrier
Devices on Polysilicon" by K.M. Panchal is a record of
work carried out under my supervision and has not been
submitted elsewhere for a degree.

Dr. S. Kar

Department of Electrical Engineering

August 7, 1980.   and

Materials Science Programme
Indian Institute of Technology,Kanpur.

Acknowledgement

I feel it my pleasant duty to express my most sincere thanks to Dr. S. Kar, who familiarized me to the field of semiconductor device technology. His patient guidence, sustained interest, and cooperation have been largely responsible for the successful completion of the present effort.

I am especially indebted to Messers S. Varma, D. Shanker, S. Bhattacharya, Rajan Varughese, and B.R. Shridhar for rendering their kind help in device fabrication and measurements. Their constructive criticism and constant encouragement were of great help throughout the course of this work.

It is a pleasure to acknowledge Dr. K.S. Chari, Miss E.A. Chakachery, and P. Saraswat for their help during various phases of this investigation.

Finally, thanks are also due to Mr. B.N. Srivastava for making neat trackings and to Miss S. Bajpai for her skillful service in typing the manuscript.

Table of Contents

A	constant, $[V^{-1}]$
A^*	effective Richardson's constant, $[A/cm^2 \; {}^{\circ}K^2]$
B	constant, $[K^{-1}]$
C	total device capacitance, $[F/cm^2]$
E_C	conduction band edge in silicon, $[eV]$
ΔE_F	Fermi level shift in grain boundary region, $[eV]$
E_{FB}	Fermi level in grain boundary region, $[eV]$
E_{FM}	Fermi level in metal, $[eV]$
E_{FS}	Fermi level in bulk silicon, $[eV]$
E_G	silicon bandgap, $[eV]$
E_0	defined by eqn. 2.5
E_{00}	defined by eqn. 2.7
E_V	valence band edge in silicon, $[eV]$
F	fill factor
h	reduced Planck's constant, $[Joule-sec]$
I	device current, $[A]$
I_D	diode current, $[A]$
I_0	diode saturation current, $[A]$
J_D	diode current density, $[A/cm^2]$
J_0	diode saturation current density, $[A/cm^2]$
J_{RT}	recombination tunneling current density, $[A/cm^2]$
J_{sc}	short circuit current density of the cell, $[A/cm^2]$
J_{TT}	thermionic tunneling current density, $[A/cm^2]$
k	Boltzmann's constant, $[eV/{}^{\circ}K]$

m^*	effective mass of electrons in semiconductor, [kg]
n	diode ideality factor
N_{doping}	doping density, [cm^{-3}]
$N_{is}(E)$	interface state density, [cm^{-2} V^{-1}]
q	electronic charge, [C]
R_S	series resistance of the solar cell, [Ohm.cm^2]
T	absolute temperature, [$^\circ$K]
$T_{ox}(V)$	oxide tunneling transmission factor
V	device voltage, [V]
V_{oc}	open circuit voltage of solar cell, [V]
V_{ox}	oxide voltage, [V]
V_{ox}^0	oxide voltage at zero bias, [V]
w	width of grain boundary, [Å]
$\emptyset_B$	Schottky barrier height, [V]
$\emptyset_B^*$	barrier height obtained from activation energy plot, [V]
$\emptyset_B^n$	Schottky barrier height for n-type silicon, [V]
$\emptyset_B^p$	Schottky barrier height for p-type silicon, [V]
$\emptyset_{BG}$	zero bias band bending at the grain boundary-bulk interface, [V]
$\emptyset_F$	Fermi potential in bulk silicon, [V]
$\emptyset_M$	metal work function, [eV]
$\emptyset_{MS}^*$	$\emptyset_M - \chi_S$, [eV]
$\emptyset_n$	$(E_c' - E_{FS}) / q$ for n-type silicon, [V]

ϕ_p $(E_V - E_{FS})/q$ for p-type silicon, [V]

φ_1 interface potential in silicon, [V]

φ_1^o interface potential in silicon at zero bias, [V]

ε_s silicon permittivity, [F/cm]

η conversion efficiency of solar cell

χ_s silicon electron affinity, [eV]

τ_T^{is} tunneling time for interface state carrier, [sec]

ABSTRACT

The present investigation has been mainly directed towards understanding the influence of grain boundaries, and other defects on carrier flow in surface barrier devices. With this in view, basically two types of studies had been carried out. One was related to investigation of carrier transport mechanisms in MOS diodes on polysilicon substrate. The other approach was to develop various techniques to characterize grain boundaries and to study their influence on electrical parameters of the device. These types of studies were useful for gaining better insight into the device operation on polysilicon material, particularly in view of the fact that MOS tunnel structures on poly-silicon can be advantageously used as photovoltaic power converters.

MOS tunnel diodes were fabricated with gold as the barrier metal on Wacker n-type polysilicon, and with alminum as the barrier metal on Wacker p-type polysilicon. The diode current-voltage characteristics and capacitance-voltage characteristics of these devices were measured over a wide range of temperature, in order to identify the dominant transport mechanism. Plots of $\ln J_o$ vs $1/T$, $1/nT$, and T were obtained and a detailed analysis was carried out. Also, for better understanding of grain boundary influences on carrier flow, a comparative study was attempted by examining conduction mechanisms in MOS diodes on single crystal silicon

substrate. The results indicated that , depending upon the presence of traps in the silicon space charge layer and the magnitude of change in band bending with temperature in silicon, the dominant transport mechanism in these devices on poly-silicon substrate could change from thermionic emission to thermionic field emission to multistep tunneling. It was also established that any hasty conclusions drawn without sufficient experimental data could lead to erroneous interpretation of the dominant mechanism.

The electrical activities of grain boundaries were investigated in polysilicon material. For Wacker polysilicon, it was found that grain boundaries had a weak influence on electrical parameters of solar cell, and the collection efficiency of photogenerated carriers was not affected much in the vicinity of grain boundaries. Large grain boundary potential barriers were not observed in Wacker polysilicon, while an examination of Monsanto polysilicon gave some indication of existence of such barriers. The results on Wacker polysilicon were quite encouraging and gave promise for efficient solar cell performance when fabricated on this material.

1. INTRODUCTION

Recent interest in the investigation of carrier transport mechanisms in MOS tunnel diodes on polysilicon stems from their potential use in inexpensive large scale terrestrial application when used as solar cells. MOS tunnel diodes with the oxide thickness in the range 15-30 Å have been used profitably as MOS solar cells [1,2]. In these devices there can be a number of carrier transport mechanisms with a different one dominating over others in different temperature ranges. Even for a given device at a particular temperature, the same mechanism may not dominate over the entire bias regime [3-6]. In polycrystalline material, grain boundaries and other structural defects can also have varied influence on the carrier flow. It is important to investigate the carrier transport mechanisms as it controls the overall performance of the cell. The mechanism which reduces the diode current but leaves the light generated current undisturbed results in a larger value of open circuit voltage than others. Also, the diode ideality factor can have different values depending upon the conduction mechanism and influence the open circuit voltage and the fill factor of the cell. For understanding and improving the performance of MOS solar cells on polysilicon, an investigation of carrier transport mechanism in these type of devices coupled with the characterization of polysilicon material is essential. It is of considerable interest to review major developments in these directions.

As these type of studies are highly interrelated, a combined study would provide better insight of the influence of grain

boundaries on electrical parameters of the cell and resolve some of the basic questions regarding the device operation on polycrystalline material.

1.1 Carrier transport mechanisms in SB/MOS diodes

An important means of gaining physical insight into the current transport mechanisms in SB/MOS devices is to study the dark current-voltage and capacitance-voltage characteristics over a wide range of temperature. Considerable amount of work, theoretical as well as experimental, has been carried out in this direction and conduction phenomena of SB/MOS devices have been clarified to some extent. Wilson [7] tried to explain the rectifying action in SB diode in terms of quantum mechanical tunneling of electrons through a barrier, but it was soon realized that this mechanism predicted the wrong direction of current flow. However, Padovani et al. [8] and later Crowell et al.[9] presented theoretical and experimental results showing that the I_D-V characteristic of Schottky barrier formed on highly doped semiconductors can be interpreted in terms of the field and thermionic field emission over a wide temperature range. These were develo ments in carrier transport model for tunneling across the barrier.

The observed direction of rectification in metal-semiconductor diodes was explained by two distinct theories namely, Schottky's diffusion theory and Bethe's thermionic emission theory. Crowell and Sze [10] developed a theory in which both of these theories were incorported into a single thermionic emission diffusion theory as a generalized model for carrier transport.

Padovani et al.[11-13] and Saxena [14] investigated the
current-voltage characteristics of Au-GaAs, Au-Si, Ni-Si,
Cr-Si systems over a wide temperature range. They empirically
found that the characteristics were dominated by a peculiar
'T_0' anomaly. 'T_0' was found to be a constant with the
dimensions of temperature and independent of voltage and
temperature over the temperature range studied. When 'T_0'
was added to the absolute temperature 'T' in the exponential
terms of the I_D-V characteristic, their experimental data was
easily explained. In this case, diode ideality factor 'n' can
be written as $n = 1 + T_0/T$ and is temperature dependent. Padovani
[15] also studied the reverse I_D-V characteristics of Au-GaAs
Schottky barrier diode above room temperature and found that ther-
mionic emission is a dominant mechanism for the reverse conduction,
but his results could not be explained by the image force
lowering theory.

Arizumi et al. [16] investigated transport properties of
Schottky barriers on silicon surface with Ag, Au, Cu as barrier
metals and reported temperature independent value of the diode
ideality factor over the temperature range 100-350 $^{\circ}$K with
'T_0' = 0. Until now no satisfactory explanation for the
observed temperature anomalies has been given.

Saxena's [14] work provided a way to distinguish between
the thermionic emission, thermionic field emission, and field
emission mechanisms of carrier transport. However, when two or
more conduction mechanisms are simultaneously responsible for
the diode current, Saxena's procedure may not be adequate to
identify the mechanism of carrier transport.

Most of the Schottky barrier diodes investigated had
invariably an oxide thickness of 10 Å. Efforts have been made
during the past few years in the direction of investigation of
carrier transport mechanisms in MOS tunnel diodes with 20-40 Å
thick oxide mainly because of their potential application in
photovoltaics. The effect of oxide thickness on various mecha-
nisms of carrier transport can be incorporated by means of an
oxide transmission coefficient [6].Kar [3,4,17] demonstrated
possible mechanisms in these devices in his experimental
investigation of the effect of oxide thickness and interface states
on the diode current in IOS tunnel diodes. It was pointed out
that thermionic emission-tunneling, recombination-tunneling via
interface states and pure tunneling from accumulation layer
could be the mechanisms which contribute to the diode forward
current at room temperature.

Recently, Tarr and Pulfrey [18] have carried out measurements
on Al-pSi MOS solar cells and reported the minority carrier
injection as the dominating transport mechanism over the
temperature range of 0-50 °C. This conclusion has been drawn
mainly on the basis of the value of activation energy (1.19 ±
0.013 eV) from the activation energy plot. In this case,
measurements of capacitance-voltage characteristics at diff-
erent temperatures were not carried out to obtain information
regarding the barrier height. Also, information regarding
barrier height and interface states from independent sources
such as small signal admittance and photoemission measurements
is essential before drawing any firm conclusion on the basis of
current-voltage characteristics only. Such type of conclusion
can be erroneous.

transport mechanism in MOS tunnel diodes on polysilicon substrate.
This is possibly due to the general belief that polysilicon may
not produce reasonable solar cell efficiencies. Now that it
is possible to achieve this, a systematic and detailed study is
to be undertaken to understand the influence of grain boundaries
on carrier flow. Kar et al. [5] have investigated carrier trans-
port mechanisms in MOS diodes fabricated on p-type Wacker poly-
silicon with aluminum barrier metal, and in SOS diodes fabricated
by chemical spraying of indium-tin oxide on n-type single cry-
stal silicon. It has been pointed out that, at room temperature,
multistep tunneling through the silicon barrier can be the
dominant transport mechanism. In these devices, slopes of
$\ln I_D$-V characteristics were found to be temperature independent
and $\ln I_0$ vs. T plot was linear. Also, the diode current was
weakly dependent on temperature. Such type of mechanism is
possible in these devices in presence of a distribution of
trap levels in the barrier region. In polysilicon material,
grain boundaries present trap levels in the barrier region,
while in SOS diodes traps may be introduced during chemical
spraying or ion beam sputtering . Such type of tunnel-assisted
transport process was detected before in case of p-n hetero-
junction [19,20], as well as in the case of ion beam sputtered
ITO on p-type silicon SOS diodes [21]. It has been pointed
out in the literature [22] that fluctuations in physical para-
meters over the diode area could cause ambiguities in the
determination of the mechanism of current transport and this
cannot be ruled out for the diodes on polysilicon substrate.

In addition to current-voltage and capacitance-voltage
measurements at different temperatures to narrow down the
probable conduction mechanisms, need arises to investigate the

these devices by seperate means. Such type of study would provide information about grain boundary potential barriers which may impede the carrier flow and determine the device characteristics.

1.2 Effects of grain boundaries in polysilicon solar cells

Grain boundaries are believed to be the most disastrous defect and plays a dominant role in determining the overall performance of the polysilicon solar cell. Various electrical activities of grain boundaries depend on a number of factors. Some of these factors can be the columnar or non-columnar nature of grain, whether a potential barrier exists at the grain boundary, and nature of the device configuration, i.e. whether pn or SB, etc.

In recent years some efforts have been made to characterize grain boundaries and to study their influence on the device performance.

Experimental work of Card et al. [23] and Seager et al. [24] involves a model which proposes the presence of potential barriers located at the grain boundaries. These barriers affect the device characteristics in various ways depending upon whether the configuration is pn or surface barrier. The effect of potential barriers at the grain boundary, on the performance of MOS solar cells has been discussed in detail by S. Bhattacharya et al. [25].

The influence of crystallographic defects and the defect-impurity complexes in p-n junction solar cells on Wacker polysilicon and EFG silicon ribbon has been studied by C.V. Hari Rao et al. [26]. The electrical activities of defects were

investigated in the scanning electron microscope operated in electron beam induced current (EBIC) mode. It was found that recombination processes in the vicinity of the grain boundary regions lead to a decrease in the electron beam induced current while twin boundaries were not found to be effective. Variation in collection efficiency of photogenerated carriers can be studied by using a photon beam scanner also. This method has an additional advantage over EBIC technique in that more detailed information can be obtained by using light sources of suitable wavelengths.

Fischer et al.[27] investigated the effect of grain size on the overall performance of the cell and pointed out the advantage of using Wacker cast polysilicon material with relatively large grain size (~150 um) and columnar structure. On this material they could achieve 10% AM1 efficiency with p-n junction configuration. Studies on p-n junction solar cells indicate, the possibility of achieving acceptable values of efficiency on polysilicon material. This shows some promise for low cost photovoltaic power generation but increased diffusion in the grain boundary region and the loss of photocarriers in the dead layer which becomes more serious in polycrystalline material sets them at a disadvantage.

Surface barrier devices have several advantages over the conventional p-n homojunction configuration such as inexpensive fabrication process, simple structure, and possibility of using less expensive material for fabrication. Low temperature processing involved in fabrication of these devices avoids degradation of minority carrier life time which is more important in polycrystalline material. Among various surface barrier configurations, the potential ability of MOS solar cells on single crystal silicon has been widely demonstrated in the past. If MOS cells on polysilicon provide

stability and acceptable value of efficiency, these cells on low cost polysilicon material will further bring down the cost of photovoltaic power generation.

MOS solar cell on Wacker cast polysilicon was first reported by Lillington and Tounsend [28]. On Al-pSi MOS with AR coating, they could obtain V_{oc} = 523 mV, J_{sc} = 22 mA/cm^2, F = 0.76 and η = 8.6% . This demonstrates that if design parameters of the cell are optimized, higher value of efficiency could be achieved. The performance of MOS solar cells on Wacker cast polysilicon has been also investigated by S. Bhattacharya et al. [29]. For MOS solar cells on n-type polysilicon with Ag barrier metal, V_{oc} = 515 mV, J_{sc} = 27.0 mA/cm^2, F = 0.71, η = 9.9% were obtained. For MOS solar cells on p-type polysilicon with Al barrier metal, V_{oc} = 467 mV, J_{sc} = 18.2 mA/cm^2, F = 0.69, η = 5.9% was obtained and no AR coating was used on these cells. The lower value of J_{sc} in case of Al barrier metal was due to higher reflection; but this can be increased with the help of AR coating. These results are encouraging. Also, it appears from the high value of fill factor that grain boundary shunting effects are negligible.

The results indicate that reasonable value of efficiency can be achieved on polysilicon surface barrier solar cells. However, in order to reduce or eliminate the unfavourable effects of grain boundaries and to realize a steady improvement in the performance of polysilicon solar cells, different techniques need to be developed to characterize grain boundaries.

1.3 Scope of the present work

The aim of the present work has been to study the carrier transport mechanisms in MOS tunnel devices on polysilicon and to investigate the influence of grain boundaries on the device performance. MOS tunnel diodes were fabricated for this purpose on Wacker cast polysilicon. Current-voltage and capacitance-voltage measurements at different temperatures in dark were carried out in order to investigate the carrier transport mechanisms in these devices. A comparative study was also attempted by examining the conduction mechanisms in the devices with identical fabrication conditions on single crystal silicon substrate to gain better understanding of grain boundary influences on the carrier flow in polysilicon material.

Various techniques were developed to characterize grain boundaries. An attempt was made to examine grain boundary potential barriers by measurements across grain boundaries. Room temperature studies on a number of dots on the solar cell arrays were taken up in order to investigate the influence of grain boundaries on the various electrical parameters of the cell. In this case, some of the dots were completely inside the grain, and others were over a varying number of perpendicular grain boundaries. The effects of grain boundaries on the light generated current were studied with a photon beam scanning arrangement. These types of studies would provide information about various electrical activities of grain boundary barriers and other defects in polysilicon material and lead to a better insight into the device operation.

2. THEORETICAL DISCUSSION

2.1 Carrier transport mechanisms in surface barrier diodes

2.1.1 Possible transport mechanisms

In case of surface barrier devices such as MOS and SOS diodes, there can be a number of carrier transport mechanisms which contribute to the diode current. In both MOS and SOS diodes, the potential barrier is formed at the silicon surface. In SOS diodes, the interface states at the oxide - degenerate semiconductor interface and located inside the degenerate semiconductor bandgap are localized while in MOS diodes states at metal - oxide interface are not localized. However, as far as the possible mechanisms of carrier transport in dark are concerned, the diodes hardly differ [5]. The energy band diagram of an MOS tunnel diode on p-type semiconductor under forward bias has been shown in Fig. 2.1. The possible carrier transport mechanisms are thermionic emission (process a), recombination tunneling via interface states (process b), thermionic field emission (process c), field emission (process d), multistep tunneling (process e), minority carrier injection (process f), and recombination in the space charge region (process g) [3-6].

2.1.2 Dependence of carrier transport mechanisms on device parameters

The forward current of an MOS tunnel diode is determined by a number of carrier transport processes (a-g). The relative magnitudes of these mechanisms depend upon various parameters, such as, barrier height, density of interface states, doping density of the semiconductor,

bias voltage, and temperature of the device [3,5]. An
oxide layer of thickness <35 Å is tunnelable to carriers.
The effect of an oxide layer on the transport mechanisms
can be taken into account by an oxide tunneling transmission
coefficient [6]. The oxide tunneling transmission coefficient
is not a constant but depends upon a number of parameters
such as : oxide composition, ϕ_{MS}^{x}, image force effect, device
voltage, oxide thickness, and density of interface states.
This has been discussed in detail elsewhere [1].

Generally in these devices, one observes that the
forward current-voltage characteristics consist of three
regions. The low bias regime is dominated by the recombina-
tion current (process g). This current is relatively more
important at low temperatures and in materials with low
life time. The high bias regime of the current-voltage
characteristic is dominated by the series resistance effect.
In the intermediate voltage regime, a number of processes
(a-f) can dominate. The carrier transport mechanism in this
bias regime is of more interest as it determines the overall
performance of the solar cell. These processes are briefly
discussed below.

Process a: In thermionic mode of carrier transport, the
majority carriers overcome the silicon barrier by pure
thermionic emission and there upon tunnel through the thin
oxide layer. In this case, the total potential barrier can
be treated separately in terms of the silicon barrier and an
oxide barrier. The resultant current density is determined
by multiplying the thermionic current over the silicon
barrier by a tunneling trranmission coefficient. The

expression for the thermionic-tunneling current density

(J_{TT}) takes the form [17]:

$$J_{TT} = T_{ox} (V) . J_O . exp (qV/nkT) \qquad (2.1)$$

Where, T_{ox} (V) is the oxide tunneling transmission

coefficient, and n is the diode ideality factor. The

expression for the diode saturation current density can

be written as:

$$J_O = A^{\overline{x}} T^2 exp (-q \varnothing_B /kT). \qquad (2.2)$$

Process b: The transition of majority carriers from the

silicon majority carrier   band into interface

states by recombination and then tunneling through the oxide

into the metal causes an excess current. The recombination

tunneling current assumes importance when either the

interface state density is high, or the thermionic tunnel-

ing current is low because of high silicon barrier or

low temperature, and at the lower values of the forward

voltage [4,30,31]. Recombination-tunneling current density

can be written as [3]:

$$J_{RT} = q \int_{E_{FM}}^{\substack{E_{FS}}} N_{is} (E) \ dE/\tau_T^{\substack{is}} \qquad (2.3)$$

Process C and Process A: Under certain circumstances, it

may be possible for the majority carriers to penetrate

the semiconductor barrier by direct tunneling. At sub-

room temperatures, thermionic-field emission (process c)

is the likely mechanism, and at low temperatures, field

emission is the likely mechanism. The upper limit of

temperature for these processes would extend further for

highly doped semiconductors. Except for very low value of forward bias, the J_D-V relationship for these mechanisms can be represented as [6]:

$$J_D = J_G \exp (V/E_0) \tag{2.4}$$

where $E_0 = E_{00} \coth (q E_{00}/kT)$ for thermionic   (2.5)
field emission,

$$= E_{00} \qquad\qquad\qquad \text{for field emission} \tag{2.6}$$

and $E_{00} = \hbar/2 (N_{doping}/m^X \varepsilon_s)^{\frac{1}{2}}$.   (2.7)

In equation(2.4), J_0 is weakly dependent on bias, and is a complicated function of temperature, barrier height, and semiconductor parameters. Under simplifying conditions, this equation reduces to the form :

$$J_G = A^X T^2 \exp (-q \phi_B/nkT), \tag{2.8}$$

for thermionic - field emission.

Process e: In presence of large number of traps in the silicon barrier r gion, multistep tunneling (process e) is a possibility. In this process, majority carriers tunnel by hopping via traps in the barrier layer. For such a mechanism, the diode current has been reported to be weakly dependent on temperature [19-21]. The forward current-voltage characteristic is expected to be of the form [19,20]:

$$J_D = J_0 \exp (AV) \exp (BT), \tag{2.9}$$

where A is a constant practically independent of voltage. In equation (2.9), $\ln J_0$ is a linear function of temperature. Such type of mechanism has been observed by several investigators [5,19-21].

Process f: Minority carrier injection can be the controlling
mechanism, if the barrier height is sufficiently large to
suppress the majority carrier flow. For this mechanism, the
current-voltage relationship can be written as:

$$J_D = J_0 \exp(qV/nkT), \qquad\qquad\qquad (2.10)$$

where $J_0 \propto T^3 \exp(-E_G/kT)$. $\qquad\qquad\qquad (2.11)$

2.1.3 Identification of dominant transport mechanisms

It can be seen from the above discussion that, the
current-voltage characteristic of an MOS tunnel diode is the
most difficult to interpret. Several mechanisms can occur in
parallel and it is very difficult to seperate and identify
a dominant mechanism contributing to the diode current in a
particular diode. An effective means to narrow down the
possible dominant mechanisms is to measure the current-
voltage and high frequency capacitance-voltage characteristics
of the device over a wide range of temperature. In addition
information about interface state density can be obtained
from small signal admittance-voltage characteristics in the
forward bias regime. But this is possible only in thicker
oxides.

From forward current-voltage characteristics at different
temperatures, J_0 can be obtained at each temperature by
extrapolation of the linear region of $\ln J_D$-V characteristic
to zero bias and plots of $\ln J_0$ as a function of T, 1/nT
can be made. If thermionic emission of majority carriers
over the top of the silicon barrier or minority carrier
injection is to be the dominant transport mechanism, then

one obtains linear ln J_D -V characteristics over a wide range of temperature with a temperature independent diode ideality factor close to unity and a linear plot of ln J_0 against 1/T [5,6,14]. If at each temperature, the value of the barrier height obtained from the $1/C^2$-V plot is close to the value of the barrier height obtained from the activation energy plot, and if it is much different from the bandgap, then the **thermionic emission** is the most likely dominant mechanism. In this case, nT is expected to be a linear function of T [14]. However, seperation between thermionic emission and minority carrier injection becomes difficult, if the value of the barrier height obtained from the activation energy plot is not much different from bandgap. One can also obtain a linear plot of ln J_0 against 1/T when recombination current dominates. But in this case, the value of the activation energy obtained is very much different from E_G and is close to $E_G/2$.

A linear ln J_D-V can also be obtained for thermionic field emission, field emission, or multistep tunneling mechanisms. If the diode current is temperature dependent, and if the plot of ln J_0 against 1/nT is linear, then thermionic field emission is the likely mechanism. In this case nT is expected to be a non linear function of T at low temperatures [14]. In case of field emission and multistep tunneling mechanisms, dependence of the diode current on temperature is negligible. For these mechanisms, the ln J_{D-V} plots at different temperatures have equal slopes, and ln J_0 varies linearly with T. The distinction between these two mechanisms becomes difficult at low temperatures. However.

at high temperatures, field emission is not probable and
multistep tunneling can be expected to be the dominant
mechanism.

The idea of taking current-voltage and capacitance-
voltage characteristics over a temperature range 77-400 $^\circ$K
often exists in literature, to identify the transport
mechanisms. However, the same mechanism may not dominate
over the entire temperature range, and there can be different
transport mechanisms in different temperature ranges.
This has been reported recently by S. Ashok et al [32].

2.2 Grain boundary studies

2.2.1 Transport across grain boundaries

Polycrystalline silicon consists of a large number of
randomly oriented grains of different size and shape which
are seperated by grain boundaries. Apart from physical
discontinuities arising from grain boundaries, other defects
such as dislocations, stacking faults, and impurities can
also be present. These defects can have varied influence
on the carrier flow. Recent reports on the measurements of
the resistivity of polysilicon proposes the presence of
potential barriers at grain boundaries [23,24]. Grain
boundary potential barriers are formed in semiconductors
because the chemical potential in the grain boundary region
is shifted from the bulk value due to the lack of perfect
periodicity. Also, depending upon the method of preparation,
the grain boundary regions may contain a large number of
point defects, impurities or other phases. This also can
result in a shift of the chemical potential.

If the grain boundary region has a lower chemical

potential for majority carriers than the bulk, then the
resultant influx of majority carriers to the boundary would
necessarily lead to the formation of a depletion region in
order for charge neutrality to be maintained and thus
creating a potential barrier. This barrier will impede normal
transport of majority carriers. However, it is quite
possible that the opposite shift of the grain boundary
chemical potential can occur, i.e., the grain boundary region
has a higher chemical potential than the bulk. In this,
case, the resultant space charge layer is an accumulation
region which has negligible influence on majority carrier
transport.

The energy band diagram of the region of an n-type
semiconductor, describing two semi-infinite grains and one
grain boundary, before and after joining has been shown in
Fig. 2.2 (a) and Fig. 2.2 (b) respectively. It has been
assumed that the chemical potential in the grain boundary
region has a lower value than the bulk of the semiconductor
grains. In equilibrium, the accumulated charge near
$x=0$ causes the energy bands to bend upwards by an amount
ΔE_F. It has been proposed that the majority carriers
overcome the barrier by thermionic emission [34,36]. In
this case, minority carriers which arrive at the barrier
edge will be transported quickly to the grain boundary.
Additional barriers can be introduced to the carrier flow
because of large perturbations of the bandgap caused by
local distortions or the presence of substantial amount of
second phase at the grain boundary. These barriers would
cause the grain boundary transport properties to differ
considerably from the simple model discussed above.

2.2.2 Effect of grain boundaries on electrical characteristics

The influence of grain boundaries on electrical parameters of the solar cell will depend upon the nature of grain boundaries. Transverse grain boundaries, which intersect the current axis of the cell, can cause a catastrophic loss in the collection of the optically generated carriers. The loss of photocarriers decreases with the grain boundary making a smaller angle with the current axis. The grain boundary will have the least effect upon the collection of photo carriers when it lies parallel to the current axis. The influence of such grain boundaries as recombination sites will be very small. Hence, the columnar nature of the individual grain is always preferred to generate acceptably efficient solar cell performance on polycrystalline substrate. The columnar grains can affect the device characteristics in various ways depending upon a number of factors. These are whether the junction is pn or a surface barrier, whether a potential barrier exists at the grain boundary, and whether the conduction along the boundary is easy or difficult. In surface barrier configuration of the solar cell, the diode current is due to the transport of majority carriers, while the light generated current is due to the transport of minority carriers. In this case, the existence of potential barriers will affect the diode and light generated current in a different manner. Suppose that the potential barrier formed is in such a way as to attract minority carriers towards the grain boundary but repel majority carriers. In this case, the diode current should not be affected unless the material contains a large number of grain boundaries. Now, if the

conduction along the grain boundary is easy then, the short
circuit current may not be altered much in the presence of
grain boundary. However, it will get reduced if the conduct-
ion along the boundary is difficult.

Now, suppose that the potential barrier formed is in
such a way as to attract majority carriers but repel minority
carriers. In this case, the short circuit current density
may not be altered much. Now, if the conduction along the
grain boundary is easy, then the diode current will increase.
This will result in a lower value of open circuit voltage
and the fill factor and will degrade the device performance.
On the other hand, if the conduction along the grain boun-
dary is difficult, the diode current may not be affected or
can even get reduced. This would lead to higher value of
open circuit voltage [25]. It can be seen that the surface
barrier solar cells are expected to perform better on poly-
crystalline substrate. In pn junction solar cells, the
diode current and the light generated current are influenced
in the same manner by the situation in the grain boundary
region. This would set them at a disadvantage.

It has been reported that grain boundary potential
barriers may not exist under illumination [37]. However,
the grain boundaries continue to act as recombination sites
and are responsible for the photovoltaic properties of poly-
silicon solar cells. Recent experiments of Seager et al.
[33,38] indicate that preferential diffusion of certain
foreign chemical species into the grain boundaries would
promote significant changes in the density of defect states
in the grain boundary regions. This can be used to advantage
in case of surface barrier solar cells.

3. EXPERIMENTAL PROCEDURE

3.1 Device fabrication

The essential steps involved in the fabrication of MOS
tunnel devices on single crystal silicon and polysilicon are
surface cleaning, growing a thin interfacial oxide layer,
evaporation of the barrier metal at the front followed by
evaporation of the back ohmic contact. In case of the device
fabrication on polysilicon to study grain boundary potential
barriers, the steps involved are surface cleaning and evaporation
of ohmic contact metal on the front surface. The fabrication
sequence of these devices is shown in Fig. 3.1. All the
fabrication steps were carried out in clean room environment.

3.1.1 Surface cleaning

Surface cleaning is the starting and critical process in
the fabrication sequence and was carried out on single crystal
and polysilicon wafers. P-type single crystal wafers (111) of
0.1-1.0 Ohm.cm. resistivity had polished front and lapped
back surface. N-type polysilicon wafers of 1.0-10.0 Ohm.cm.
resistivity and p-type polysilicon wafers of 1.0-10.0 Ohm.cm.
resistivity were obtained from Wacker Chemitronic. Monsanto
p type polysilicon wafers of 0.1-0.3 Ohm.cm. resistivity were
also used for making devices. The grains were of different
shapes and dimensions varied between 1 and 8 mm. Surface cleaning
included degreasing with organic solvents followed by chemical
etching with acids. The wafers were cleaned in a clean chemical
bench, and all solvents and acids used were of electronic grade.
Chemical etching was found to be the most critical step for the
removal of damaged layer from the surface of polysilicon. For

polycrystalline material, steps followed in sequence were as
follows.

(i)   The wafer was degreased by treating in warm trichloroethy-
      lene for about 2 minutes and then in warm acetone for 2
      minutes to remove traces of trichloroethylene followed by
      warming in methanol for removing traces of acetone.

(ii) The wafer was then chemically polished by etching in a
      mixture of CP4 and HNO_3 (1:1) for 2 minutes to remove the
      damaged surface layer from either side.

(iii) The wafer was rinsed in deionized water several times to
      remove traces of acids.

      For Monsanto wafer, chemical polishing resulted in
unsmooth wafer surface and step (ii) was replaced by etching in
HF to remove any oxide layer present on the wafer surface.

      The cleaning of single crystal silicon involved step
(i) as mentioned above followed by the steps below.

(ii) The wafer was etched in HF to remove the intrinsic oxide.

(iii) The wafer was rinsed in deionized water several times to
      remove traces of HF.

(iv) This was followed by treating the wafer in warm HNO_3 for
      about 5 minutes to grow an oxide about 50-60 A^o thick.

(v)   The wafer was rinsed in deionized water several times to
      remove traces of HNO_3.

(vi) The wafer was etched in HF again to remove freshly grown
      oxide.

(vii) Finally, the wafer was rinsed several times in deionized
      water to remove traces of HF.

Steps (iii) (v) were necessary to avoid chemical etching of the surface which would damage the flatness of the surface.

After this surface cleaning process, the wafer surface came out hydrophobic and was ready for further processing.

3.1.2 Oxidation

Immediately after chemical cleaning of the wafer, a thin interfacial layer of oxide was grown at a high temperature in dry oxygen. The oxidation was carried out in a horizontal flow, open end 60 mm i.d. fused silica tube in a three zone Thermco Spartan furnace. Dry oxygen was bubbled through a liquid nitrogen trap before admitting into the furnace tube. After loading, the wafer was kept at the mouth of the tube for a short time to dry the wafer surface completely before moving into the hot zone. The oxide was grown at a temperature of 700 °C and at an oxygen pressure of 1.0 atmosphere for 60 seconds. The oxygen flow rate was more than 1.0 litre/min. For these oxidation conditions, the thickness of the oxide layer was found to be 20 Å [30]. The oxide of this thickness is tunnelable to carriers and has been reported to be optimum for the solar cell performance [1,2].

3.1.3 Metallization

The metallization was carried out in an oil free high vacuum system (Grainville Phillips Co. USA, series 252) having a digital quartz crystal thickness monitor (Perkin Elmer, USA, Model 605-1210). To minimize oil contamination liquid nitrogen traps were used with rotary and diffusion pumps.

For evaporation of aluminum and gold, tungsten helical filament was used. A tungsten conical basket was used for silver evaporation. The metals evaporated were obtained in form of wires, 1.0 to 1.5 mm in diameter and had 5N purity. The tungsten filaments were thoroughly degreased in warm trichloroethylene, acetone, and methanol, and were then outgassed in

vacuum by passing igher current than that required for
evaporation of met ls. The metals were degreased in the same
procedure used for fil ments and degassed before an evaporation.
At the time of degassing, a shutter was kept between the source
and the substrate in order to prevent contamination of the
substrate surface by any foreign volatile species coming out.
To ensure a uniform film and to reduce substrate heating, the
source to substrate distance was kept more than 10 cm.

On n-type silicon Au, Ag were used as barrier metals and
Al was used for the ohmic contact. On p-type silicon, Al was
used as barrier metal and Au, Al were used as ohmic contact
metals. The choice of barrier metals and ohmic contact metals
have been discussed in detail elsewhere [1].

MOS tunnel diodes with thick metal layer were fabricated
on polysilicon as well as on single crystal silicon in order to
study carrier transport mechanism. Thick circular dots of
0.4 and 0.5 mm diameter of the barrier metal were deposited
through molybdenum masks on the front surface. This was followed
by deposition of ohmic contact metal on the back surface. The
rate of deposition for the back contact and thick dot was kept
above 10.0 $\overset{o}{A}$/sec.

Thin metal layer deposition was carried out on poly-
silicon for studying the photovoltaic behaviour of MOS tunnel
diodes with polysilicon as substrate and arrays contained some
dots inside the grain and others located over varying number
of grain boundaries. Metal layer thickness was in the range
of 50 to 120 $\overset{o}{A}$ and the deposition rate between 1.0 and 6.0
$\overset{o}{A}$/sec. Also, large area solar cells with diameter 5 to 7 mm

were fabricated on polysilicon and were used in the photon beam
scanning analysis.

Arrays consisting of 0.4 and 0.5 mm diameter dots were
also made on polysilicon to study grain boundary barriers.
Thick circular dots of Al were evaporated through molybdenum masks
on one surface of the n-type wafer and an Al strip about 1 mm
in width was evaporated near the edge of the wafer. Au was evap-
orated similarly on p-type polysilicon. The choice of the metal
was dictated by the fact that this should form ohmic contact
on polysilicon, for any barrier formation would otherwise
obscure the effects of grain boundary potential barrier.

The chamber pressure was kept well below $1.0x10^{-5}$ torr
during all evaporations.

3.2. Measurements

3.2.1 Measurements at different temperatures

A simple heating arrangement consisting of two polished
brass discs with a heating element wound on a mica sheet in
between was employed. This was fitted closely in a hollowed
out teflon block. The device was mounted in a shielded, light
tight box, on a gold plated brass disc, which formed one
contact terminal. The temperature of the disc was accurately
measured with the help of a chromel-alumel thermocouple and a
Leeds and Northrup type 8691 millivolt potentiometer. The
temperature of the disc was controlled precisely within
± 0.5 °C by a temperature controller. The front contact on the
device was made with the help of a telescopic spring probe with
a very sharp tip. Care was taken to prevent any lateral
movement of the block after the front contact was made. The

current-voltage and capacitance-voltage measurements were carried out in dark at various values of temperatures.

3.2.1.1 Current-Voltage Measurements

The circuit diagram used for the measurement of diode current at different values of bias is shown is Fig. 3.2 (a). Measurements were carried out in dark. The diode current as a function of applied bias was plotted on a semilogarithmic graph. The diode ideality factor n was obtained from the slope of the linear region of the forward ln I_D-V characteristic using the relation n=(q/kT) (dV/d $\ln I_D$). The reverse saturation current I_0 was obtained by extrapolating the linear region of the forward ln I_D-V plot to zero bias. This was used to determine the barrier height. The series resistance was obtained from the linear range of the I_D-V characteristic.

3.2.1.2 Capacitance-Voltage Measurements

The capacitance-voltage characteristics were measured at 100 kHz using the set up shown in Fig. 3.2 (b). The a.c. signal voltage of the capacitance bridge was kept below 15 mV peak-to-peak to avoid any inaccuracy due to the non linear charge-voltage relation of the device.

The device capacitance was measured at regular bias intervals up to considerably large reverse bias values. The plot of reciprocal of the squared capacitance as a function of bias was a straight line. The doping density and the zero bias silicon band bending were obtained from the slope of the straight line and the intercept on the bias axis, respectively, by using the relations [1,40]:

$$N_{doping} = 2/(r.\varepsilon_s.\ln(1/C^2)/dV),\qquad (3.1)$$

$$\varphi_1^o = V_{intercept} - (kT/q)\,\text{for n-type},\qquad (3.2a)$$

$$\varphi_1^o = -V_{intercept} + (kT/q)\,\text{for p-type}\qquad (3.2b)$$

The zero bias barrier height was obtained according
to the relations:

$$\phi_B^n = \varphi_1^o + \phi_n,\qquad (3.3a)$$

$$\phi_B^p = \varphi_1^o + \phi_p.\qquad (3.3b)$$

3.2.2 Studies on grain boundary effects

Various techniques were developed for characterizing
grain boundaries.

To study the effect of grain boundaries on the
electrical parameters of the solar cell on polysilicon,
current-voltage and capacitance-voltage measurements were
carried out at room temperature in dark on number of dots
in the cell array. Measurements were made on the dots
located over a single grain and a varying number of grain
boundaries. The device was mounted in a shielded, light
tight box, on a water cooled copper block which formed one
contact terminal. The other contact was made to the dots
with the help of a very sharp tip telescopic probe. During
measurements under illumination, the box cover was uncovered.
The procedure for current-voltage and capacitance-voltage
measurements has been discussed in 3.2.1.1 and 3.2.1.2,
respectively. For the same dots, the values of open circuit
voltage and short circuit current density under AMI

illumination was also e sured. AMI illumination was
simulated with the help of a 150 W tungsten lamp and checked
with the help of a commercial OCLI p-n junction solar cell.

A photon beam scanning arrangement was set up to study
the effect of grain boundaries and other imperfections on the
light generated current of the solar cells on polysilicon.
Optics of this arrangement is shown in Fig. 3.3. This consisted
essentially of an arrangement to focus the light coming from
a collimated source to a very fine beam of less than 0.5 mm
in diameter. The focused beam was made to fall over the solar
cell mounted on a gold plated copper block, stationed on the
micropositioner platform of the microscope with X-Y movement
capability enabling one to move the device in the X or Y
direction relative to a stationary light beam. Two spring
probe attachment was provided to make contact on the sample.
The photon-beam-induced current was measured as the sample
was scanned by a light beam. The grain structure of the device
was viewed through a microscope.

Grain boundary potential barriers were examined by
measuring the current-voltage characteristics across the grain
boundary. The arrangement for mounting the device and making
contact was the same as described above. Contacts were made
on the strip and the dot or between two dots so that only one
grain boundary was incorporated between them. Measurements
of current-voltage characteristics were carried out in dark
and ploted on a linear graph. Next, two or more grain
boundaries were incorporated between the contacts and the same
measurements were repeated.

4. RESULTS AND DISCUSSIONS

4.1 Studies of carrier transport mechanisms

4.1.1 MOS diodes on single crystal silicon

MOS diodes with aluminum as the barrier metal were fabricated on p-type single crystal silicon wafers with bulk resistivity of 0.1 to 1.0 Ohm. cm. The oxide thickness was about 20 $\overset{o}{A}$. The back ohmic contact was gold for all these devices. Forward current-voltage characteristics of these devices were measured in dark at different temperatures spanning the range: 294 to 414 ^{o}K. Corresponding high-frequency measurements were also carried out in dark. Temperature of the device was controlled accurately with a temperature controller, and the maximum error involved in temperature measurements was $\pm$ 0.5 ^{o}C. The measured current voltage characteristics at different temperatures have been presented in Fig. 4.1. Corresponding C^{-2}-V characteristics are shown in Fig. 4.4. The important experimental data obtained from these measurements have been listed in Table 4.1 for a representative device. The doping density, calculated from the slope of C^{-2}-V characteristics correspond to the bulk resistivity data obtained on this material. The bulk Fermi level $\emptyset_F$ was calculated from the experimentally obtained doping density. The device area was measured under a microscope.

It can be seen from Table 4.1 that with increasing temperature, the zero bias band bending φ^o_1 decreases and the value of bulk Fermi potential $\emptyset_F$ increases. According to the energy band diagram given in Fig. 2.1,

$$\varphi_1^O = (E_G + \chi_s - \emptyset_M)/q - V_{ox}^O - \emptyset_F.$$

A part of change in φ_1^O with temperature can be
accounted by the change in the bandgap E_G and the bulk
Fermi level $\emptyset_F$. It is also expected that the work function
of the metal and the electron affinity of silicon would
change with temperature, although there does not seem to
be any experimental data to support this [6]. It may
be noted that, over the entire temperature range the
total change in zero bias silicon bandbending, $\Delta\varphi_1^O$, is 0.12V,
whereas $(E_G/q - \emptyset_F)$ is 0.10 V, cf., Table 4.1.
Hence, $\Delta\varphi_1$ can be, more or less explained by the change
in the bandgap and the bulk Fermi level with temperature.
Attempts can be made to relate the change in the interface
state charge with the change in the Fermi level position.
But, this would lead to contradiction of the experimental
results. Experimentally, $(\varphi_1^O + \emptyset_F)$ has been found to
decrease with temperature (cf., Table 4.1). This would
mean that the Fermi level at higher temperature will be
farther away from the conduction band edge at the Si-SiO$_x$.
interface. The result is that the interface state charge
becomes less negative due to a change in occupancy of
the interface states. This would cause a decrease in the
oxide potential V_{ox}^O which should lead to an increase in
$(\varphi_i^O + \emptyset_F)$. This is in contradiction with the observed
behaviour of $(\varphi_i^O + \emptyset_F)$ with temperature. The $\ln I_D$-V
characteristics of the device exhibit fairly good
exponential behaviour over 2-3 decades of current,

cf., Fig. 4.1. Recombination and interface recombination-tunneling components seem to be negligible. The diode ideality factor n has been obtained from the slope of the linear region of the $\ln I_D$-V characteristic. The value of n is more or less constant except for the highest temperature, 414 $^\circ$K. The extrapolation of the linear region of the $\ln I_D$-V characteristics to ero bias gives the reverse saturation current at each temperature . The corresponding current densities listed in Table 4.1 have been used to obtain activation energy plots of $\ln J_o$ vs 1/T and 1/nT. These plots have been presented in Fig. 4.2. It can be seen that both plots are equally linear. However, the value of the barrier height obtained from the $\ln J_o$ vs 1/nT plot comes out to be 1.08 V, whereas the value obtained from $\ln J_o$ vs 1/T plot is 0.76 V. It can be seen that the value of the barrier height obtained from the $\ln J_o$ vs 1/nT plot is more close to the value of $(\varphi_i^o + \emptyset_F)$, cf., Table 4.1. The relation for thermionic emission can also be used to calculate the value of the barrier height $\emptyset_B$ from the intercept of the linear region of the forward $\ln I_D$-V characteristic, assuming that the carrier transmission coefficient through the oxide is unity. However, it may be observed from Table 4.1 that while $(\varphi_i^o + \emptyset_F)$ decreases with temperature, $\emptyset_B$ increases. Fig. 4.17 contains plot of nkT/q vs kT/q and it is evident from the nature of the plot that thermionic emission is the likely mechanism [14]. The variation of $\ln J_o$ vs T has been presented in Fig. 4.3. The non linear relationship observed between $\ln J_o$ and T

indicates that the field emission is not the probable
mechanism of carrier transport in this device.

4.1.2 MOS diodes on polysilicon

4.1.2.1 MOS diodes on p-type polysilicon

The measured forward current-voltage characteristics of
a typical MOS device Al 25 P C3 on p-type polysilicon, are
presented in Fig. 4.5. Corresponding $1/C^2-V$ characteristics
are shown in Fig. 4.8. Measurements were taken for the
device temperatures of 294, 314, 334, 354, 374, 394, and
414 ^{O}K. The diode had gold as the back ohmic contact. The
interfacial layer thickness was about 20 $\overset{O}{A}$. The results of
measurements on this device have been summarized in Table
4.2. The behaviour of φ_i^O, $\emptyset_F$, and $(\varphi_i^O + \emptyset_F)$ with temperature
is similar to what has been observed in the case of MOS
diodes on p-type single crystal silicon. In this case,
the total change in zero bias band bending between 294 and
394 ^{O}K is 0.23 V, whereas $/(E_G/q-\emptyset_F)$ is 0.10 V, cf.,
Table 4.2. It can be seen that the total change in φ_i^O can
only
/be partially accounted by the corresponding change in
E_G and $\emptyset_F$. Also, as has been discussed in sec. 4.1.1,
the behaviour of φ_i^O with temperature cannot be explained
by change in the interface states occupancy due to the
shift in the bulk Fermilevel. The $\ln I_D-V$ characteristics
of Fig. 4.5 indicate an exponential behaviour over 2-3
decades. The value of the diode ideality factor n is
found to be constant except for the highest temperature
at which the device characteristic might have undergone

a change due to constant heating. In Fig. 4.6, $\ln J_o$ has been plotted as a function of $1/T$ and $1/nT$. It can be seen that the plot of $\ln J_o$ vs $1/nT$ is linear, whereas the plot of $\ln J_o$ vs $1/T$ deviates from linearity. The value of the barrier height obtained from $\ln J_o$ vs $1/nT$ plot comes out to be 1.04 V, which is close to the value of $(\varphi_i^o + \emptyset_F)$, cf., Table 4.2. For this device, the plot of $\ln J_o$ vs T is linear. This is some indication of the presence of a tunneling component contributing to the diode current. However, from Fig. 4.17, it can be seen that the plot of nkT/q vs kT/q is linear. This indicates that pure tunneling is not the dominant transport mechanism [14].

It should be noted that, in presence of a tunneling component, the value of barrier height $\emptyset_B$, obtained (cf., Table 4.2) from Eq. 2.2 by assuming thermionic emission as the dominant mechanism, may not represent the true value.

4.1.2.2 MOS diodes on n-type polysilicon

Studies have been conducted on Au n-Si MOS diodes on polysilicon substrate and the experimentally observed values of various parameters of two typical diodes have been summarised in Tables 4.3 and 4.4. These devices had an interfacial layer thickness of about 20 Å and the back ohmic contact was aluminum.

Figures 4.9 and 4.12 represent the $\ln I_D$-V and $1/C^2$-V characteristics, respectively, of device Au 76 P B3 at device temperatures of 298, 316, 336, 357, 376, 396, and 415 °K. In Figs. 4.13 and 4.16 are presented the $\ln I_D$-V and $1/C^2$-V characteristics, respectively, of device Au 56 P B5 at device temperatures of 307, 327, 345, 365, 385,

Table 4.3 contains the important experimental data for the device Au 76 P B3. The variation of φ_1^O, $\emptyset_F$, and $(\varphi_1^O + \emptyset_F)$ with temperature ollows similar trend as observed for MOS diodes. Since $\varphi_1^O = (\emptyset_M - \chi_s)/\hat{q} - V_{ox}^O - \emptyset_F$ for n-type semiconductor, a part of change in φ_1^O with temperature can be explained as due to a corresponding change in the bulk Fermi level $\emptyset_F$. However, this does not completely account for the total change in φ_1^O, i.e. $\wedge \varphi_1^O = 0.16$ V, whereas $-\emptyset_F$ is only 0.09 V, cf., Table 4.3.

For this device, the general features of the $\ln I_D$-V characteristics and the nature of $\ln J_O$ vs T^{-1}, $1/nT$, and T plots, are similar to those of device Al 25 P C3. The diode ideality factor is found to be temperature independent.

Table 4.4 lists the data obtained from $\ln I_D$-V and $1/C^2$-V characteristics on device Au 56 P B5. For this device, $\wedge \varphi_1^O = 0.28$ V, in the temperature range 307 to 425 ^{O}K. This change is very large and can not be accounted by the shift in the Fermi level with temperature.

The $\ln I_D$-V characteristics presented in Fig. 4.13 do not follow the trend as has been observed in case of devices Al 1 B2, Al 25 P C3, and Au 76 P B3. An unusual feature of these characteristics is that the slope is temperature independent. Thermionic emission of majority carriers over the silicon barrier or minority carrier injection is not the probable transport mechanism because of the following reasons. First, the diode ideality factor is much higher than 1.0 and depends strongly on temperature.

Second, a plot of $\ln J_o$ vs T^{-1} has been found to be
strongly non-linear, indicating that an activation energy
is not involved in the dominant mechanism of carrier trans-
port. Also, for minority carrier injection, much smaller
values of J_o can be expected for moderately doped
semiconductors. Thermionic field emission is also ruled
out, because nT is independent of temperature and $\ln J_o$ vs
1/nT is a vertical plot [14]. This leaves field emission
through the silicon barrier as the possible transport
mechanism. This conclusion can be arrived at because of the
fact that, ln J_o vs T plot is linear, and nT is independent
of temperature [14,1º]. However, for moderately doped
semiconductors, and at high device temperatures, field
emission is not the probable mechanism [6]. This type of
behaviour has been observed by several workers [5,19-21].
It has been suggested that, in presence of large number of
traps in silicon barrier region, multistep tunneling is a
                                    is assumed to be dominant,
probable mechanism. If this mechanism/ then from Eq.2.9,
the values of A and B come out to be 18 V^{-1} and 0.04 K^{-1},
respectively. In comparision, for Al p-Si MOS diodes on
polysilicon, the value of A obtained was 22 V^{-1} and that
of B was 0.052 K^{-1} [5]. For SOS diodes fabricated by
chemical spraying of ITO on n-type silicon, the value of
A obtained was 23 V^{-1} and that of B was 0.05 K^{-1} [5].
This indicates that, the values of A and B obtained for
device Au 56 P B5 do confirm to the reported values. For

multistep tunneling process, φ_1^0 is responsible for the change in I_D with temperature [21]. It can be seen that $\Delta \varphi_1^0$ between 307 to 425 °K is 0.28 V, cf., Table 4.4, whereas the corresponding voltage displacement in the $\ln I_D$-V characteristics is 0.26 V, cf., Fig. 4.13. Hence the change in I_D with temperature can be explained by $\Delta \varphi_1^0$. The existance of a large number of **trap** levels in polysilicon can arise due to the presence of grain boundaries, dislocations and other defects.

Table 4.1: Experimentally obtained values of various parameters of an MOS device Al 1 B2

T ($^{\circ}$K)	φ_i^o (V)	N_{doping} (cm^{-3})	Φ_F (V)	$\varphi_i^o + \Phi_F$ (V)	J_o (A cm^{-2})	n	nT ($^{\circ}$K)	Φ_B (V)	Φ_B^V (V)
294	0.96	2.16×10^{16}	0.16	1.12	2.1×10^{-9}	1.33	391	0.91	
313	0.94	2.22×10^{16}	0.17	1.11	2.1×10^{-8}	1.34	419	0.91	
334	0.92	2.22×10^{16}	0.18	1.10	1.2×10^{-7}	1.33	444	0.93	1.08
354	0.90	2.28×10^{16}	0.19	0.09	6.5×10^{-7}	1.33	470	0.94	
374	0.88	2.28×10^{16}	0.20	1.08	2.4×10^{-6}	1.32	494	0.95	
394	0.86	2.31×10^{16}	0.21	1.07	8.4×10^{-5}	1.31	576	0.96	
414	0.84	2.31×10^{16}	0.22	1.06	2.4×10^{-5}	1.28	530	0.98	

The area of this device was 1.2×10^{-3} cm^2.

Table 4.2: Experimentally obtained values of various parameters of nMOS device Al 25 P C3.

T (°K)	φ_i^0 (V)	N_{doping} (cm^{-3})	Φ_F (V)	$\varphi_i^0 + \Phi_F$ (V)	J_o (A cm^{-2})	n	nT (°K)	Φ_B (V)	Φ_B^* (V)
294	0.80	6.27×10^{15}	0.19	0.99	9.8×10^{-9}	1.29	379	0.87	
314	0.76	6.42×10^{15}	0.20	0.96	6.7×10^{-8}	1.29	404	0.89	
334	0.72	6.42×10^{15}	0.21	0.93	3.8×10^{-7}	1.29	430	0.90	1.04
354	0.66	6.42×10^{15}	0.22	0.88	2.0×10^{-6}	1.29	455	0.90	
374	0.62	6.47×10^{15}	0.24	0.86	1.1×10^{-5}	1.28	480	0.90	
394	0.57	6.47×10^{15}	0.25	0.82	4.3×10^{-5}	1.28	506	0.91	
414	0.54	6.52×10^{15}	0.26	0.80	7.4×10^{-4}	1.60	662	0.86	

The area of this device was 1.2×10^{-3} cm^2.

Table 4.3: Experimentally obtained values of various parameters of an MOS device Au 76 P B2.

T ($^{\circ}K$)	φ_1^{o} (V)	N_{doping} (cm^{-3})	Φ_F (V)	$\varphi_1^{o} + \Phi_F$ (V)	J_o (A cm^{-2})	n	nT ($^{\circ}K$)	Φ_B (V)	$\Phi_B^{\#}$ (V)
298	0.60	2.94×10^{15}	0.23	0.83	2.7×10^{-7}	1.32	393	0.81	
316	0.57	3.46×10^{15}	0.25	0.82	4.6×10^{-7}	1.31	414	0.84	
336	0.54	3.59×10^{15}	0.26	0.80	2.4×10^{-6}	1.31	440	0.85	0.90
357	0.51	3.73×10^{15}	0.28	0.79	1.0×10^{-5}	1.31	468	0.86	
376	0.48	4.04×10^{15}	0.30	0.78	4.1×10^{-5}	1.31	493	0.87	
396	0.46	4.41×10^{15}	0.31	0.77	1.4×10^{-4}	1.31	519	0.87	
415	0.44	5.11×10^{15}	0.32	0.76	4.8×10^{-4}	1.32	543	0.87	

The area of this device was 7.9×10^{-3} cm^2.

Table 4.4: Experimentally obtained values of various parameters of an MOS device Au 56 P B5

T ($^{\circ}K$)	φ_i^o (V)	N_{doping} (cm^{-3})	Φ_F (V)	$\varphi_i^o + \Phi_F$ (V)	J_o ($A\ cm^{-2}$)	n	nT ($^{\circ}K$)	Φ_B (V)
307	0.66	1.95×10^{15}	0.25	0.91	5.6×10^{-6}	2.14	657	0.75
327	0.60	2.12×10^{15}	0.27	0.87	1.1×10^{-5}	2.01	657	0.78
345	0.54	2.32×10^{15}	0.29	0.83	2.2×10^{-5}	1.90	556	0.81
365	0.50	2.63×10^{15}	0.30	0.80	5.1×10^{-5}	1.80	657	0.83
385	0.42	2.83×10^{15}	0.32	0.74	1.0×10^{-4}	1.71	658	0.86
405	0.41	3.82×10^{15}	0.32	0.73	2.4×10^{-4}	1.62	556	0.88
425	0.38	4.78×10^{15}	0.34	0.72	5.3×10^{-4}	1.54	655	0.89

The area of this device was 1.3×10^{-3} cm^2.

4.2 Grain boundary studies

4.2.1 Transport across grain boundaries

Studies have been carried out to investigate grain
boundary potential barriers in Wacker polysilicon and
Monsanto polysilicon material. The bulk resistivity of
Wacker p-type and n-type polysilicon wafers was 1.0-10.0
Ohm. cm., while for Monsanto p-type it was 0.1-0.3 Ohm.
cm. Figs. 4.18 and 4.19 display current-voltage character-
istics for typical devices fabricated on Wacker n-type
and p-type polysilicon, respectively. The ohmic contact
metal was gold for p-type polysilicon and aluminum for
n-type polysilicon. The I-V measurements were carried
out by incorporating different number of grain boundaries
between contacts. These characteristics show essentially
an ohmic behaviour regardless of the number of grain
boundaries inbetween contacts. The resistance involved
is of the order of 100 Ohms which can nearly be accounted
for by the bulk resistivity of the material. This shows
that the grain boundaries in Wacker polysilicon are devoid
of large barriers resulting from uncompensated charge.

' Fig. 4.20 depicts the I-V characteristics of
a representative device on Monsanto p-type polysilicon.
Silver was used as an ohmic contact metal. The I-V
characteristics show ion-ohmic behaviour in high bias
region. It can be seen that current across grain boundary
decreases as the number of grain boundaries incorporated
in between contacts increases. This can be due to the
effect of grain boundary potential barriers on the carrier
transport. Very high resistance in the linear region of

I-V characteristics has been observed. It can also be noted that the I-V characteristics are asymmetric and asymmetry exists even in case of two contacts without any grain boundary incorporated inbetween them. According to the simple model described in sec. 2.2.1 for carrier transport across grain boundary, this may not be due to grain boundary potential barrier. However, the transport properties of carriers can be considerably modified by the existance of additional barriers in the material arising due to various impurities and other defects, which are incorporated during the growth process. Also, it is probable that silver may be forming a low barrier on p-type poly-silicon.

4.2.2 Effect of grain boundaries on electrical character-
istics

Tables 4.5 and 4.6 contain representative experimental data obtained from MOS solar cells on n-type polysilicon with gold and silver as barrier metals. A number of cell arrays consisting of 0.5, and 1.0/dots have been fabricated to study the influence of grain boundaries on device parameters. The thickness of the barrier metal layer was varied between 50 and 120 Å. The contact was made to the dots with the help of a very sharp tip telescopic probe. The values of short-circuit current density, fill factor, and conversion efficiency of the cell could not be determined accurately because of the shadowing effect of the probe. The measured $\ln I_D$-V and $1/C^2$-V characteristics

of various dots in array Au 56 P, have been displayed in Fig. 4.21
and 4.22, respectively. Figures 4.23 and 4.24 depict the measured
lnI_D-V and $1/C^2$-V characteristics of various dots in array Ag 32 P.
It is evident from Tables 4.5 and 4.6 that there is a weak influen-
ce of grain boundaries on open circuit voltage. However, in presen-
ce of large number of grain boundaries and defects, the value of
open circuit voltage is considerably lower. The diode ideality
factor seems to be higher in presence of grain boundaries. This
may be due to higher value of recombination currents and a larger
density of interface states [25]. The value of series resistance
is not affected much by the grain structure. It can be observed
that the value of barrier height obtained from $1/C^2$-V characteristr-
ics decreases with increasing number of grains, cf., Tables 4.5,
and 4.6. This has also been reflected in the values of the barrier
height obtained from the I_D-V data of array Ag 32 P, cf., Table
4.6. However, for array Au 56 P, the values of the barrier height
obtained from the I_D-V data do not follow any particular trend,cf.,
Table 4.5. It can be noticed that the large values of barrier
height and nice I_D-V characteristics are obtained on Wacker poly-
silicon. It may be expected that the grain boundaries will influence
the collection efficiency of the photogenerated carriers. The
influence of grain boundaries and other defects as recombination
sites has been studied by a photon beam scanning arrangement. Large
area MOS solar cells with diameter 5 to 7 mm have been fabricated
on Wacker n-type polysilicon with gold and silver as barrier metals.
The thickness of the barrier metal layer was varied between 50 and
320 Å. The photon-beam-induced current was measured /as the sample was

scanned by a very fine beam of light of less than 0.5
mm in diameter. The variation of the light generated current
observed has been about 7 to 9 percent in the region of
large number of grain boundaries, while it was about 2 to 4
percent in the region of one or two grain boundaries. It can
be noticed that the defect contribution to device performance
by recombination mechanism is not pronounced for Wacker
polysilicon material. This also has been observed earlier
by C.V. Hari Rao et al [26].

Table 4.5: Influence of grain boundaries on various parameters of MOS polysilicon cells.

Device No. [Dot]	Dot located on	Dot Area (cm^2)	V_{oc} (mV)	Rs (Ohm. cm^2)	n	N_{doping} (cm^{-3})	Φ_F (V)	φ_1^o (V)	$\varphi_1^o + \Phi_F$ (V)	Φ_B (V)
Au 56I										
E3	1 grain	2.0×10^{-3}	373	0.47	1.50	1.67×10^{15}	0.25	0.64	0.89	0.77
B2	2 grains	2.0×10^{-3}	378	0.38	1.50	1.67×10^{15}	0.25	0.65	0.90	0.90
D1	2 grains + twin boundaries + defects	2.0×10^{-3}	376	0.52	1.66	1.36×10^{15}	0.26	0.62	0.88	0.78
D5	3 grains + twin boundaries	1.3×10^{-3}	362	0.46	1.66	1.18×10^{15}	0.26	0.60	0.86	0.76
B5	4 grains	1.3×10^{-3}	368	0.39	1.58	1.67×10^{15}	0.25	0.60	0.85	0.80

The polysilicon material was n-type (Wacker Chemitronic) and had a bulk resistivity of 1.0-10.0 Ohm. cm. Surface etching was carried out in a mixture of CP4 and HNO_3 (1:1) for two minutes. Dry oxidation was carried out at 700°C for 60 seconds.

Table 4.6: Influence of grain boundaries on various parameters of MOS polysilicon cells.

Device No. [Lot]	Dot located on	V_{oc} (mV)	R_s (Ohm. cm^2)	n	N_{doping} (cm^{-3})	Φ_F (V)	φ_i^o (V)	$\varphi_i^o + \Phi_F$ (V)	Φ_B (V)
Ag 32P									
.33	1 grain	387	0.21	1.33	1.92×10^{15}	0.25	0.67	0.92	0.88
A3	3 grains	384	0.18	1.42	1.94×10^{15}	0.25	0.62	0.87	0.85
B1	4 grains	390	0.18	1.50	1.83×10^{15}	0.25	0.64	0.89	0.85
C2	5 grains + twin boundaries	370	0.21	1.58	1.95×10^{15}	0.25	0.60	0.85	0.82

The polysilicon material was n-type (Wacker Chemitronic) and had a bulk resistivity of 1.0 - 10.0 Ohm. cm. Surface etching was carried out in a mixture of CP4 and HNO_3 (1:1) for two minutes. Dry oxidation was carried out at 700 °C for 60 seconds. The dot area was 7.9×10^{-3} cm^2.

5. CONCLUSIONS

MOS diodes were fabricated both on single crystal and polysilicon substrates with an interfacial layer thickness of about 20 $\mathring{A}$. The barrier metal was Au on n-type silicon, and Al on p-type silicon. The carrier transport mechanisms in these devices were investigated by carrying out measurements of diode current-voltage characteristics and capacitance-voltage characteristics at various temperatures. The activation energy analysis was carried out by plotting $\ln J_0$ as a function of $1/T$, and $1/nT$. Plots of $\ln J_0$ vs T were also made. In all these devices, the values of silicon band bending at zero bias, obtained from $1/C^2-V$ characteristics showed a decrease with increasing temperature. In Al MOS diodes on p-type single crystal silicon, the change in φ_i^0 with temperature was more or less explained by decrease in the bandgap, and shift in the Fermi level position. However, in MOS diodes on polysilicon substrate, it was observed that the total change in φ_i^0 over the temperature range of study, was larger than that observed in case of Al MOS diodes on single crystal silicon. This change in φ_i^0 could not be accounted for by the decrease in the silicon bandgap and the change in bulk Fermi level with temperature. From, experimental data, $(\varphi_i^0 + \emptyset_F)$ was also found to decrease with increasing temperature. This behaviour of $(\varphi_i^0 + \emptyset_F)$ could not be explained by considering the change in interface state charge with the change in Fermi level position with temperature.

In case of Al MOS diodes on p-type single crystal silicon, $\ln J_o$ vs $1/T$ and $1/nT$ plots were found to be equally linear. The variation of $\ln J_o$ with temperature was a non linear function. This indicated the absence of field emission component. Also, the nature of nkT/q vs kT/q plot revealed that thermionic emission may be the dominant transport mechanism. However, the value of the barrier height obtained from the saturation current value, assuming thermionic emission, was found to increase with temperature. This was quite opposite to the behaviour of $(\varphi_1^o + \emptyset_F)$ with temperature. The results indicated the difficulty encountered in analysizing results. One common feature observed in devices on polysilicon was that, the $\ln J_o$ vs T plot was always linear. This indicated the presence of a tunneling component in MOS diodes fabricated on polysilicon. In case of Al MOS diodes on p-type polysilicon, and in one set of Au MOS diodes on n-type polysilicon, $\ln J_o$ was found to be linear with respect to $1/nT$ rather than $1/T$. This together with the nature of $\ln J_o$ vs $1/T$ and $\ln J_o$ vs $1/nT$ plots showed that thermionic field emission could be the dominant transport mechanism. The nature of nkT/q vs kT/q plots might lead one to believe that, thermionic emission could be the dominant mechanism. However, it should be noted that in presence of thermionic field emission, the plot of nkT/q vs kT/q deviates from linearity in low temperature range. But, at higher temperatures, the nature of this plot does not differ from that for observed in the thermionic emission. An unusual feature was $\ln I_D$-V

characteristics of some Au MOS diodes on polysilicon. The following typical behaviour was noticed for these devices. The decrease in φ_1^O was very large, and nT was constant rather than n. Also , the plot of $\ln J_O$ vs $1/T$ was strongly non linear. The variation of $\ln J_O$ with T was linear. From the nature of these plots and experimental data, it was concluded that thermionic emission, thermionic field emission, or minority carrier injection could not be the dominant transport mechanism. In these devices, the change in I_D with temperature could be explained by the corresponding variation of $\Delta \varphi_1^O$. The observed behaviour in these devices was similar to what had been noticed by several workers earlier [5,19-21], and indicated the possibility of multistep tunneling through the silicon space charge layer as the dominant transport mechanism in presence of large number of traps in polysilicon material. From the experimental data collected , and on the basis of theoretical discussion, it became clear that the dominant transport mechanism could depart from thermionic emission to thermionic field emission to multistep tunneling depending upon the magnitude of $\Delta \varphi_i^O$ and presence of traps in the silicon space charge layer. The study also stressed that sufficient caution should be exercized before drawing any firm conclusion about the dominant carrier transport mechanism. The study of grain boundary potential barriers revealed that, Wacker polysilicon material is devoid of large potential barriers. The measured I-V characteristics showed an ohmic behaviour, and the resistance involved was accounted for by the bulk resistivity of the material. Similar studies on Monsanto polysilicon material indicated the

possible existance of grain boundary potential barriers.
From the studies carried out to investigate the influence
of grain boundaries on electrical parameters of solar cell,
it was found that the grain boundaries had only a weak
influence on open circuit voltage, diode ideality factor,
series resistance, and barrier height in silicon. Similar
results had been reported earlier by S. Bhattacharya et al
[25]. The influence ofgrain boundaries on photogenerated
carriers was investigated by a photon beam scanning arrange-
ment, and it was observed that the variation of light
generated current was not significant in grainboundary regions.
These types of studies established that, MOS structures with
their inherent advantages over p-n junction configuration,
could be used profitably on Wacker polysilicon material
for photovoltaic applications.

List of References

1. S. Kar et al,'Fabrication of Silicon MOS solar cells', Annual Report, Project No. CEL/DE/76-77/35, I.I.T. Kanpur (1977).

2. S. Bhattacharya, M.Tech. Thesis, I.I.T. Kanpur (1978).

3. S. Kar and W.E. Dahlke, 'Potentials and direct current in Si · (20 to 40 $\overset{O}{A}$) SiO_2 · Metal Structures', Solid State Electron. 15, 869 (1972).

4. S. Kar, 'Characterization of silicon MOS tunnel diodes', IEDM Technical Digest, 79, IEEE (NY) (1976).

5. S. Kar, S. Ashok and S.J. Fonash,'Evidence of tunnel assisted transport in non-degenerate MOS and SOS diodes at room temperature', J. Appl. Phys. 51 (6), 3417 (1980).

6. E.H. Rhoderick, Metal - Semiconductor Contacts, Clarendon Press, Oxford (1978)

7. A.H. Wilson, Proc. Roy. Soc. A 136, 487 (1932).

8. F.A. Padovani and R. Stratton,'Field and Thermionic-Field emission in Schottky barriers', Solid State Electron. 9, 695 (1966).

9. C.R. Crowell and V.L. Rideout,'Normalized Thermionic-Field emission in metal-semiconductor (Schottky) barriers', Solid State Electron. 12, 89 (1969).

10. C.R. Crowell and S.M. Sze,'Current transport in metal-semiconductor barriers', Solid State Electron. 9, 1035 (1966).

11. F.A. Padovani and G.G. Sumner,'Experimental Study of Gold-Gallium Arsenide Schottky barriers', J.Appl. Phys. 36 (12), 3744 (1965).

12. F.A. Padovani, 'Graphical determination of the Barrier Height and Excess temperature of a Schottky Barrier', J. Appl. Phys. 37, 921 (1966).

13. F.A. Padovani, 'Forward voltage-current characteristics of Metal-Silicon Schottky Barriers', J. Appl. Phys. 38, 891 (1957).

14. A.N. Saxena, 'Forward current-voltage characteristics of Schottky barrier on n-type Si', Surface Science. 13, 151 (1969).

15. F.A. Padovani, 'Thermionic emission in Au-GaAs Schottky Barriers', Solid State Electron. 11, 193 (1968).

16. Tetsuya Arizumi and Masataka Hirose, 'Transport properties of Metal-Silicon Schottky barriers', J. Appl. Phys. 8 (6), 749 (1969).

17. S. Kar, 'On the role of interface states in MOS solar cells', J. Appl. Phys. 49 (10), 5278 (1978).

18. N.G. Tarr and D.L. Pulfrey, 'New experimental evidence for minority-carrier MIS diodes', Appl. Phys. Lett. 34 (4), 295 (1979).

19. J.P. Donnelly and A.G. Milnes, 'Current/Voltage characteristics of p-n Ge-Si and Ge-GaAs heterojunctions', Proc. IEE 113 (9), 1468 (1966).

20. A.R. Riben and D.L. Feucht, 'n Ge-p GaAs heterojunctions', Solid State Electron. 9, 1055 (1966).

21. W.S. Chang and J.R. Sites, 'Electronic characterization of indium tin oxide/silicon photodiodes', J. Appl. Phys. 49 (9), 4833 (1978).

22. G.S. Visweswaran and R. Sharan, 'Current transport in large area Schottky Barrier Diodes', Proc. IEEE 67 (3), 436 (1979).

23. H.C. Card and E.S. Yang, 'Electrical processes at grain boundaries in polycrystalline semiconductors under optical illumination', IEEE Trans. Electron Devices ED 24 (4), 397 (1977).

24. C.H. Seager and T.G. Castner,' Zero bias resistance of grain boundaries in neutron transmutation doped polycrystalline silicon', J. Appl. Phys. 49 (7), 3879 (1978).

25. S. Bhattacharya, S. Varma and S. Kar, 'Effects of barrier metal, optical concentration and grain boundary on polysilicon MOS solar cells', IEDM Technical Digest, 430, Washington D.C. (1979).

26. C.V. Hari Rao, R.O. Bell, M.C. Cretella, J.C. Ho, F.V. Vald and K.V. Ravi,'Response of defects to illumination in silicon solar cells', Proc. 13th IEEE Photo. Spec. Conf., 1213 (1978).

27. H. Fischer and W. Pschunder, 'Low Cost Solar Cells based on large area unconventional silicon', Proc. 12th IEEE Photo. Spec. Conf., 86 (1976).

28. D.R. Lillington and W.G. Tounsend,'Cast polycrystalline Schottky-barrier solar cells', Appl. Phys. Lett. 31, 471 (1977).

29. S. Bhattacharya, D. Shanker, S. Varma, and S. Kar, 'MOS Solar cells on polycrystalline silicon', Digest of Tech. Papers, 11th International conference on Solid State Devices, 219, Tokyo (1979).

30. S. Kar, D. Shanker, S.P. Joshi, and S. Bhattacharya, 'Experimental and theoretical study of silicon MOS solar cells with different Barrier Metals', Proc. 13th IEEE Photo. Spec. Conf., 86 (1976)

31. S. Kar,'Effects of interface states, tunneling and metal in silicon MOS solar cells', IEDM Tech. Digest, 56A, Washington D.C. (1977).

32. S. Ashok, J.M. Borrego, and R.J. Gutmann, 'Electrical characteristics of GaAs MIS Schottky Diodes', Solid State Electron. 22, 621 (1979).

33. C.H. Seager, D. S. Ginley, J.D. Zook, 'Improvement of Polycrystalline Silicon Solar Cells with grain boundary hydrogenation techniques', Appl. Phys. Lett. 36 (10), 31 (1980).

34. J.Y.W. Seto,'The electrical properties of polycrystalline silicon films', J. Appl. Phys. 46, 5247 (1975).

35. H.F. Matare, Defect Electronics in Semiconductors, John Wiley, New York: 1971.

36. H.F. Matare,'Enhanced Carrier Collection at grain boundary barriers in solar cells made from large grain polycrystalline material', Solid State Electron, 22, 651 (1979).

37. H. Paul Maruska, Amal K. Ghosh, Albert Rose, and Tom Feng, 'Hall mobility of Polycrystalline Silicon', Appl. Phys. Lett. 36 (5), 381 (1980).

38. C.H. Seager and D.S. Ginley,'Passivation of grain boundaries in Polycrystalline Silicon', Appl. Phys. Lett. 34 (5), 337 (1979).

39. S. Kar and D. Shanker, To be Published.

40. S.M. Sze, Physics of Semiconductor Devices,
    Wiley, New York (1969).

FIGURE CAPTIONS

Fig. 2.1   Energy band diagram of an MOS diode on p-type silicon.

Fig. 2.2   Energy band diagram describing two semi-infinite silicon grains and one grain boundary

(a) before joining,

(b) after joining.

Fig. 3.1   Sequence of the fabrication steps for various devices.

Fig. 3.2   Circuit diagram of the set-up used for measuring

(a) diode current-voltage characteristics,

(b) capacitance-voltage characteristics.

Fig. 3.3   Arrangement for photon beam scanning.

Fig. 4.1   Measured diode current-voltage characteristics of MOS diode Al 1 B2 at different temperatures.

Fig. 4.2   Experimental plots of $\ln J_0$ vs $1/T$ and $1/nT$ for MOS diode Al 1 B2.

Fig. 4.3   Experimental plot of $\ln J_0$ vs T for MOS diode Al 1 B2.

Fig. 4.4   Measured $1/C^2$ vs V characteristics of MOS diode Al 1 B2 at different temperatures.

Fig. 4.5   Measured diode current-voltage characteristics of MOS diode Al 25P C3 at different temperatures.

Fig. 4.6   Experimental plots of $\ln J_0$ vs $1/T$ and $1/nT$ for MOS diode Al 25P C3.

Fig. 4.7   Experimental plot of $\ln J_0$ vs T for MOS diode Al 25P C3.

Fig. 4.8   Measured $1/C^2$ vs V characteristics of MOS diode Al 25P C3 at different temperatures.

Fig 2 1

Fig 2 2 a

Fig 2 2 b

Fig 3 1

Variable voltage DC power supply APLAB LVA 30/2

Digital voltmeter Yamuna 1010

Sample box

DC Ammeter

Temperature controller

Fig 3 2 a

Temperature controller

Digital voltmeter Yamuna 1010

Sample box

AC Milli voltmeter APLAB M 2

Capacitance Bridge Boonton 94 C - S 18

Hi

Lo

Fig 3 2 b

Fig 3 3

Fig 4 1

Fig 4,2

Device A1 B2
p Si, Al

J_C
(A/cm^2)

T (°K)

Fig 4 3

Fig 4 4

Device A. 25 F C3
F Polysilicon, Al

T(°K)

◇   294
◆   314
□   334
■   354
△   374
●   394
○   414

Fig 4 5

Fig 4 6

Fig 4 7

Fig 4 8

Device Al 25P C 3
p Polysilicon, Al

T(°K)
◇ 294
◆ 314
□ 334
■ 354
△ 374
● 394
○ 414

V(V)

C^{-2}
$(F^{-2}.10^{21})$

Fig 4 9

Fig 4 10

Fig 4 11

Device Au 76P B2
n Polysilicon, Au

T(°K)	
298	◇
316	◆
336	□
357	■
376	▽
396	●
415	○

C^{-2} $(F^{-2} 10^{20})$

V (V)

Fig 4 12

Fig. 4 13

Fig 4 14

Fig 4.15

Device Au 56P B 5
n Polysilicon, Au

T(°K)	
307	◇
327	◆
345	□
365	■
385	△
405	●
425	○

Fig 4 16

C^{-2}
$(F^{-2} \ 10^{21})$

V (V)

Device Au 56 P B 5
Au, Polysilicon

△ AL1 B 2
■ AL 25 PC 3
○ Au 76P B 2
● Au 56 P B 2
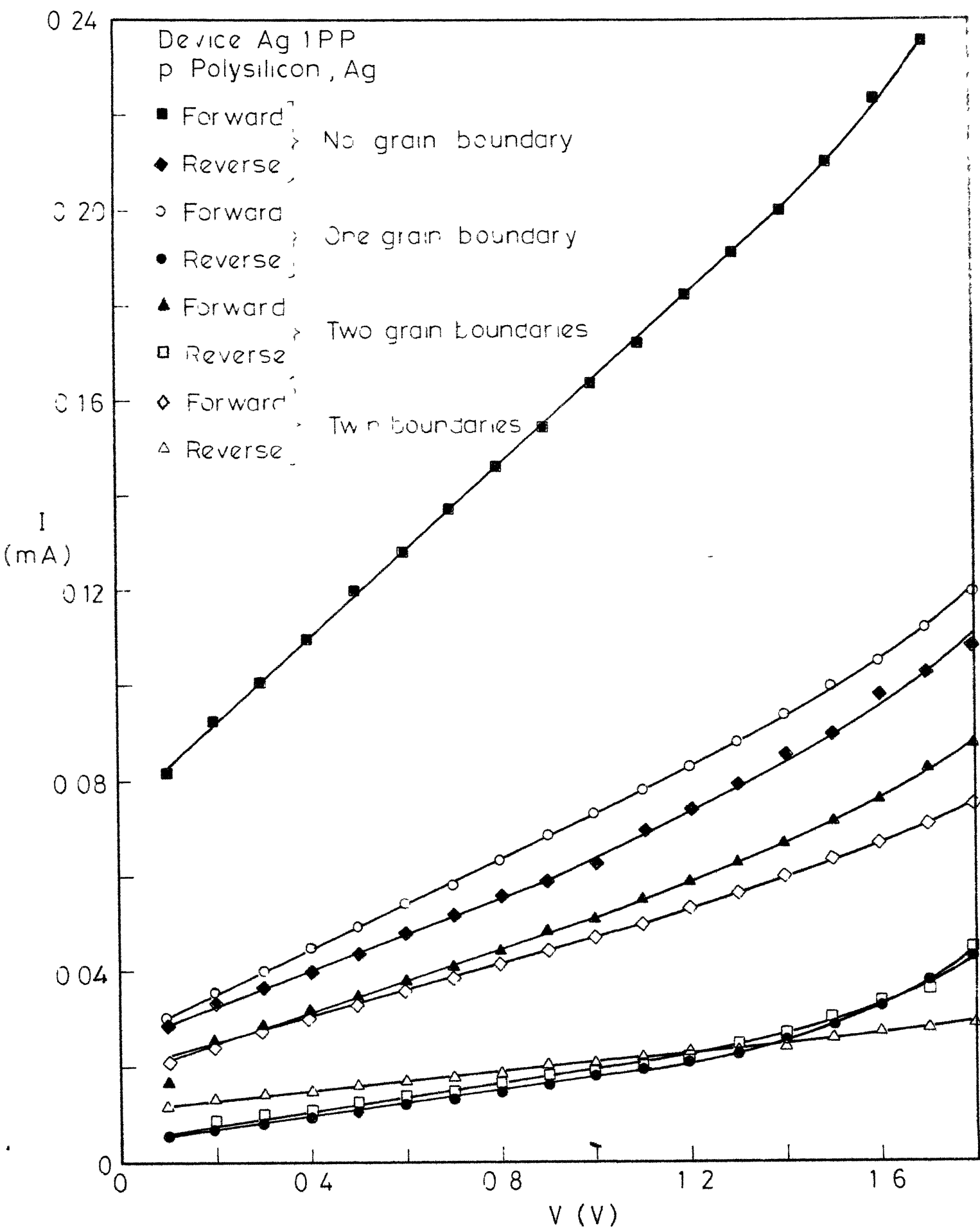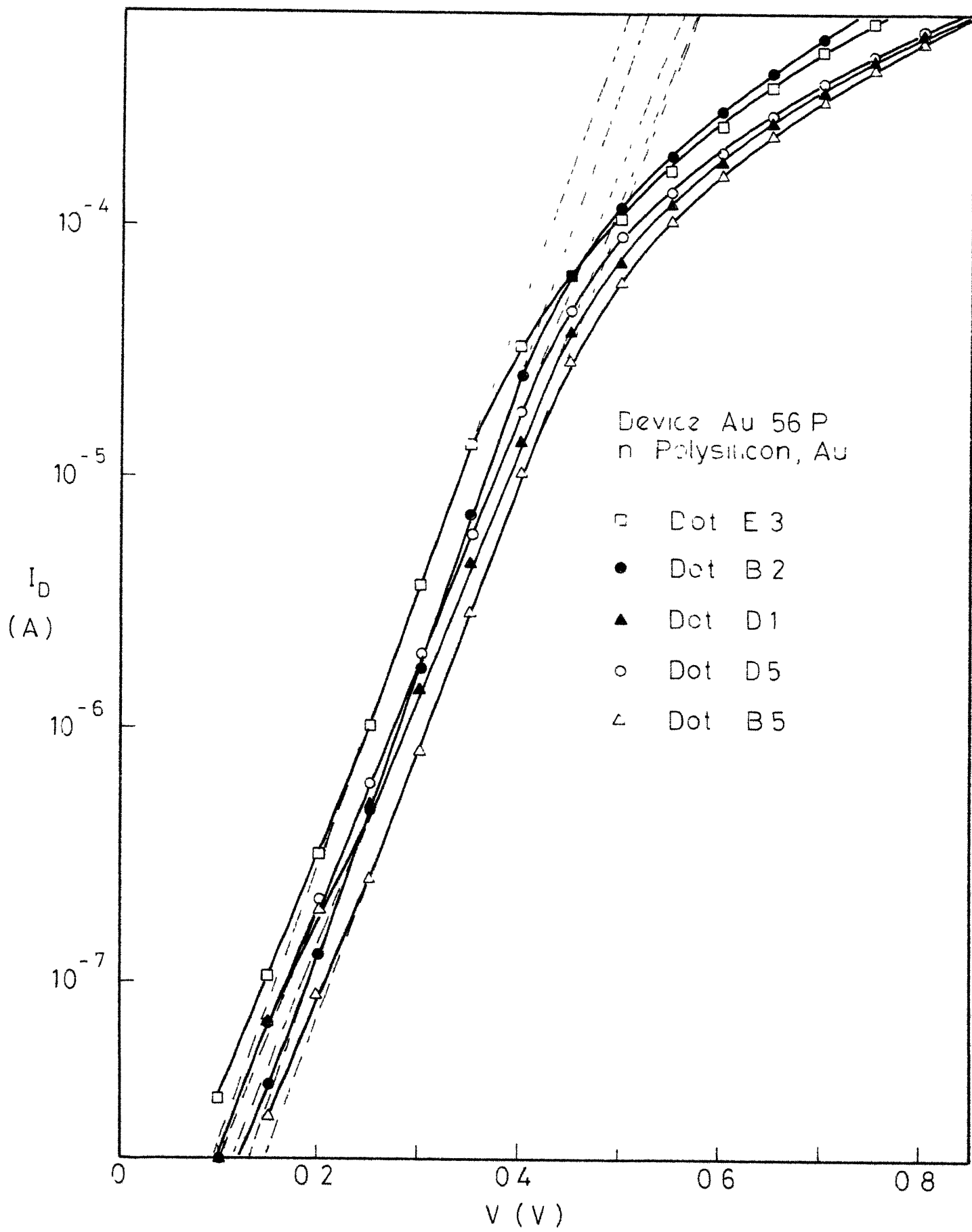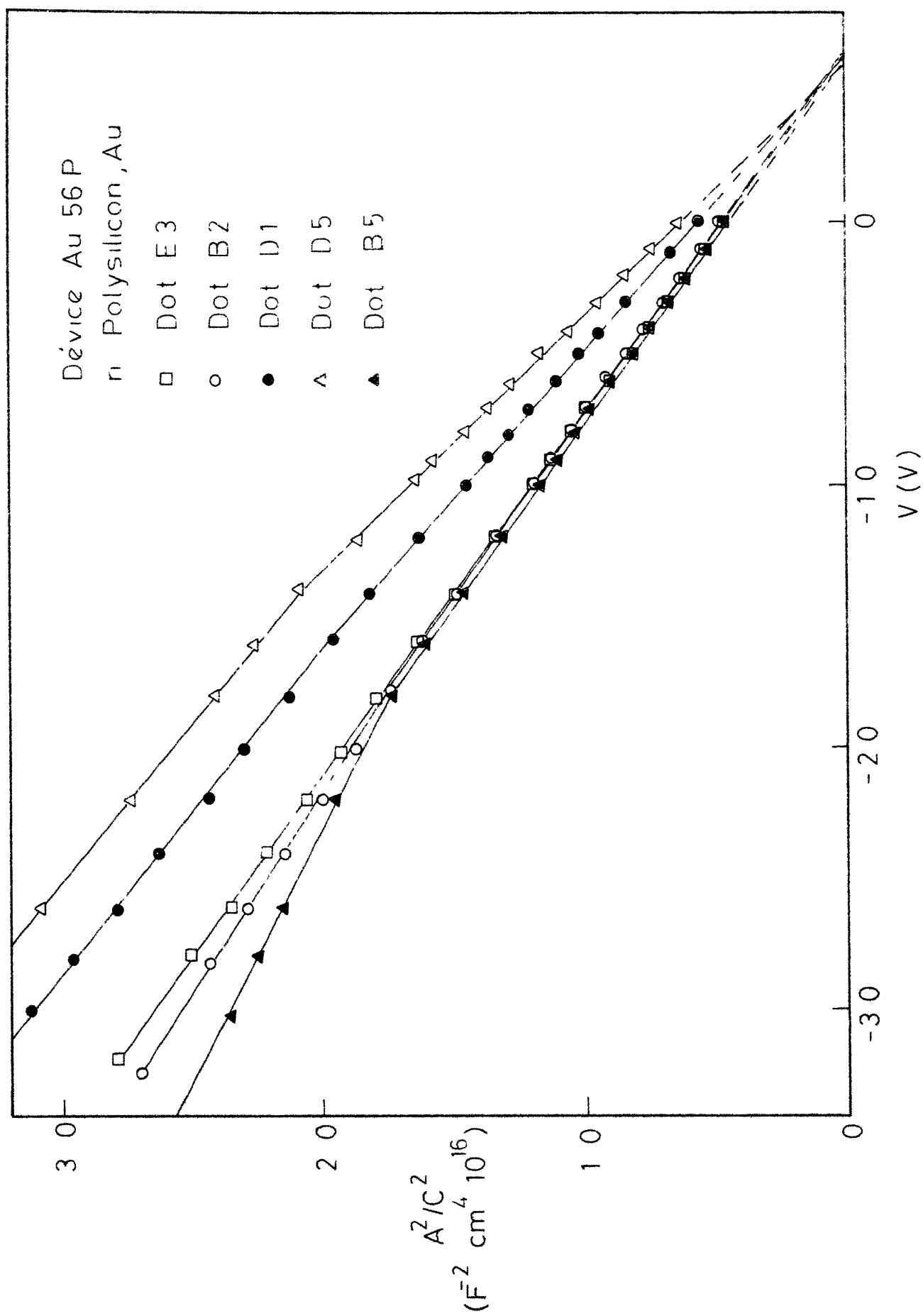
nkT/q
(mV)

600

400

200

0

-10.0

100   200   300   400

kT/q (mV)

Fig 4 17

Fig 4.18

Fig 4 19

Fig 4 20

Fig 4 21

Fig 4 22

Dévice Au 56 P

n Polysilicon, Au

□   Dot E 3

○   Dot B 2

●   Dot D 1

▽   Dot D 5

▲   Dot B 5

V (V)

$\frac{A^2}{C^2}$

$(F^{-2} cm^4 10^{16})$

Fig 4 23

Device Ag 32P
n Polysilicon, Ag

Dot B 3 ▲
Dot A 3 ●
Dot B 1 ○
Dot C 2 □

Fig 4 24

V (V)

$(F^{-2} \ C^{-2} \ 10^{20})$